



OIST

OKINAWA INSTITUTE OF SCIENCE AND TECHNOLOGY GRADUATE UNIVERSITY
沖縄科学技術大学院大学

Ran-GTP Is Non-essential to Activate NuMA for Mitotic Spindle-Pole Focusing but Dynamically Polarizes HURP Near Chromosomes

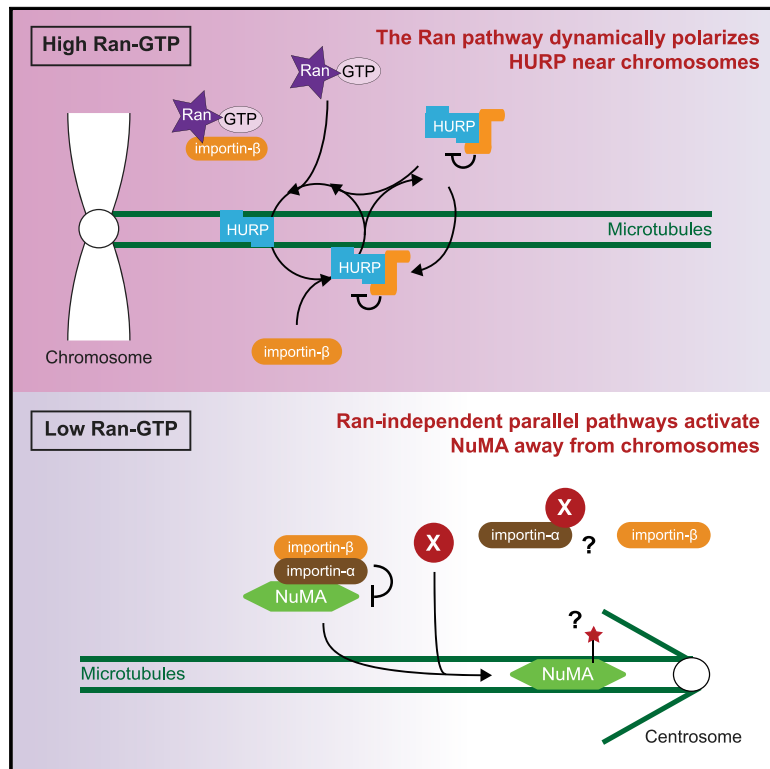
Author	Kenta Tsuchiya, Hisato Hayashi, Momoko Nishina, Masako Okumura, Yoshikatsu Sato, Masato T. Kanemaki, Gohta Goshima, Tomomi Kiyomitsu
journal or publication title	Current Biology
volume	31
number	1
page range	115-127.e3
year	2020-11-12
Publisher	Elsevier Inc.
Rights	(C) 2020 The Author(s).
Author's flag	publisher
URL	http://id.nii.ac.jp/1394/00001699/

doi: [info:doi/10.1016/j.cub.2020.09.091](https://doi.org/10.1016/j.cub.2020.09.091)

Current Biology

Ran-GTP Is Non-essential to Activate NuMA for Mitotic Spindle-Pole Focusing but Dynamically Polarizes HURP Near Chromosomes

Graphical Abstract



Authors

Kenta Tsuchiya, Hisato Hayashi, Momoko Nishina, ..., Masato T. Kanemaki, Gohta Goshima, Tomomi Kiyomitsu

Correspondence

tomomi.kiyomitsu@oist.jp

In Brief

Tsuchiya et al. develop acute mitotic depletion assays using auxin-inducible degron technology to dissect Ran's mitotic roles in human HCT116 cells. This study shows that Ran-GTP is non-essential to activate NuMA away from chromosomes but is required to activate HURP near chromosomes.

Highlights

- Using AID technology, we developed mitotic depletion assays for the Ran pathway
- The Ran pathway is non-essential to activate NuMA for spindle-pole focusing
- Ran-GTP is not required to target TPX2 but is required to localize HURP and HSET
- The Ran pathway maintains HURP's polarized spindle localization during metaphase



Article

Ran-GTP Is Non-essential to Activate NuMA for Mitotic Spindle-Pole Focusing but Dynamically Polarizes HURP Near Chromosomes

Kenta Tsuchiya,^{1,6} Hisato Hayashi,^{1,6} Momoko Nishina,^{1,6} Masako Okumura,^{1,6} Yoshikatsu Sato,¹ Masato T. Kanemaki,^{2,3,4} Gohta Goshima,¹ and Tomomi Kiyomitsu^{1,2,5,7,*}

¹Division of Biological Science, Graduate School of Science, Nagoya University, Chikusa-ku, Nagoya 464-8602, Japan

²Precursory Research for Embryonic Science and Technology (PRESTO) Program, Japan Science and Technology Agency, 4-1-8 Honcho Kawaguchi, Saitama 332-0012, Japan

³Department of Chromosome Science, National Institute of Genetics, Research Organization of Information and Systems (ROIS), Yata 1111, Mishima, Shizuoka 411-8540, Japan

⁴Department of Genetics, SOKENDAI (The Graduate University of Advanced Studies), Yata 1111, Mishima, Shizuoka 411-8540, Japan

⁵Okinawa Institute of Science and Technology Graduate University, 1919-1 Tancha, Onna-son, Kunigami-gun, Okinawa 904-0495, Japan

⁶These authors contributed equally

⁷Lead Contact

*Correspondence: tomomi.kiyomitsu@oist.jp

<https://doi.org/10.1016/j.cub.2020.09.091>

SUMMARY

Spindle assembly is spatially regulated by a chromosome-derived Ran-GTP gradient. Previous work proposed that Ran-GTP activates spindle assembly factors (SAFs) around chromosomes by dissociating inhibitory importins from SAFs. However, it is unclear whether the Ran-GTP gradient equivalently activates SAFs that localize at distinct spindle regions. In addition, Ran's dual functions in interphase nucleocytoplasmic transport and mitotic spindle assembly have made it difficult to assess its mitotic roles in somatic cells. Here, using auxin-inducible degron technology in human cells, we developed acute mitotic depletion assays to dissect Ran's mitotic roles systematically and separately from its interphase function. In contrast to the prevailing model, we found that the Ran pathway is not essential for spindle assembly activities that occur at sites spatially separated from chromosomes, including activating NuMA for spindle-pole focusing or for targeting TPX2. On the other hand, Ran-GTP is required to localize HURP and HSET specifically at chromosome-proximal regions to set proper spindle length during prometaphase. We demonstrated that Ran-GTP and importin- β coordinately promote HURP's dynamic microtubule binding-dissociation cycle, which maintains HURP near chromosomes during metaphase. Together, we propose that the Ran pathway acts on spindle assembly independently of its interphase functions in mitotic human cells but does not equivalently regulate all Ran-regulated SAFs. Ran-dependent spindle assembly is likely coupled with additional parallel pathways that activate SAFs distantly located from the chromosomes.

INTRODUCTION

During cell division, a microtubule-based spindle structure is assembled around chromosomes to efficiently capture and segregate duplicated chromosomes into daughter cells.^{1,2} Spindle assembly is dependent on a gradient of a guanosine triphosphate (GTP)-bound form of Ran (Ran-GTP), which surrounds chromosomes in animal cells.^{3,4} Ran-GTP is produced by regulator of chromosome condensation 1 (RCC1), a guanine nucleotide exchange factor (GEF) for Ran,⁵ and is hydrolyzed to Ran-guanosine diphosphate (GDP) by RanGAP1, a GTPase-activating protein for Ran.⁶ As RCC1 and RanGAP1 mainly localize on chromosomes and in the cytoplasm, respectively, these opposing enzymes create a chromosome-derived Ran-GTP gradient after the nuclear envelope breaks down (Figure 1A). After mitotic exit, RCC1 still binds to chromatin although RanGAP1

localizes to the nuclear envelope and the cytoplasm. Thus, these enzymes generate different Ran-GTP concentrations in the nucleus and cytoplasm, which drives nucleocytoplasmic transport during interphase.⁴ The Ran-GTP gradient has been best characterized in *Xenopus* egg extracts,^{7,8} but is also found in other meiotic and mitotic cell types.^{9–11} Recent studies indicate that Ran-GTP is essential for acentrosomal spindle assembly in female meiosis,^{9,12,13} but the significance of Ran-GTP in mitotic spindle assembly has been debated.^{10,11,14}

Similar to the mechanisms of nucleocytoplasmic transport,⁴ Ran-GTP binds to importin- β during mitosis, thereby releasing inhibitory importins from spindle assembly factors (SAFs) near chromosomes (Figure 1A).^{15–18} Once activated, most SAFs interact with microtubules and spatially regulate microtubule nucleation, dynamics, transport, and cross-linking, which in turn creates specialized local structures of the spindle.^{3,4} For



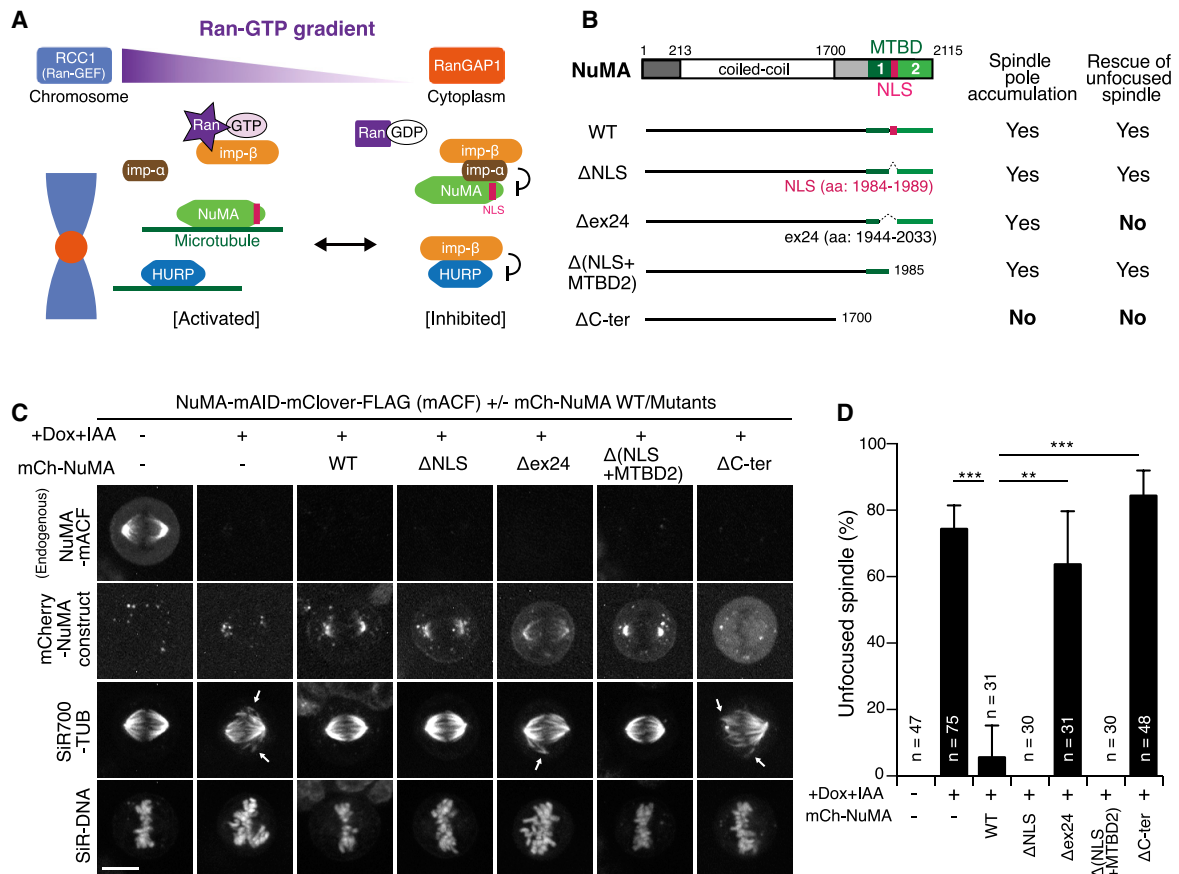


Figure 1. NuMA Acts in Spindle-Pole Focusing Using Its Conserved Microtubule-Binding Domain

(A) The prevailing model of SAF inhibition and activation.

(B) Full-length NuMA and truncation fragments.

(C) Live fluorescence images of metaphase NuMA-mACF cells 24 h after treatment with Dox and IAA. Arrows indicate unfocused microtubules.

(D) Quantification of unfocused spindles for each condition in (C) from 3 independent experiments. p values were calculated using Dunnett's multiple comparisons test after one-way ANOVA ($F(3,6) = 33.81$; $p = 0.0004$).

See also Figure S1. Error bars indicate mean \pm SD; * $p < 0.05$, ** $p < 0.01$, *** $p < 0.001$, **** $p < 0.0001$; scale bars, 10 μ m.

instance, nuclear mitotic apparatus protein (NuMA) recognizes the minus ends of microtubules and transports and cross-links microtubules in cooperation with cytoplasmic dynein to focus and maintain spindle microtubules at the poles in mammalian cells.^{19–22} The targeting protein for Xklp2 (TPX2) is required for spindle pole organization^{23,24} and stimulates microtubule nucleation in a Ran- and importin- α -regulated manner.^{25–28} Kinesin-14 human spleen, embryo, and testes expressed (HSET/XCTK2) cross-links both parallel and anti-parallel microtubules near chromosomes but preferentially cross-links parallel microtubules near the spindle poles.^{29–31} Hepatoma upregulated protein (HURP) accumulates on microtubules near chromosomes to form bundled kinetochore microtubules (k-fibers).³² Most SAFs, including NuMA, TPX2, and HSET, contain a nuclear localization sequence/signal (NLS),^{29,33,34} which is specifically recognized by importin- α (Figure 1A). On the other hand, some SAFs, such as HURP, are directly recognized by importin- β (Figure 1A).³²

NuMA was first described as a Ran-importin-regulated SAF in *Xenopus* egg extracts^{15,16} (Figure 1A) together with TPX2.¹⁷ We

now know that, in mitotic human cells, NuMA localizes to the spindle poles and the polar cell cortex, where it facilitates spindle-pole focusing and astral microtubule capture/pulling, respectively.^{19,20,35} Recently, Chang et al.³³ solved a crystal structure of the importin- α -NuMA-NLS complex, illustrating that NuMA's microtubule-binding activities are inhibited by steric blockage of importin- β *in vitro*. However, how Ran-GTP activates NuMA in cells has not been rigorously examined.

To understand the mechanisms and significance of Ran-based regulation of SAFs, it is critical to separate Ran's mitotic roles from its interphase nucleocytoplasmic transport function. To achieve this, we developed mitotic depletion assays for the Ran pathway in human cells by combining mitotic drugs with auxin-inducible degron (AID) technology,³⁶ which allows us to degrade mAID-tag fusion proteins with a half-life of 20 min. In contrast to the prevailing model, we found that depletion of RCC1, RanGAP1, or importin- β , even during mitosis, does not substantially affect the localization and function of NuMA at the spindle poles. However, we also found that Ran-GTP is required to localize HURP and HSET near chromosomes.

Overall, our studies indicate that the Ran pathway acts on spindle assembly separately from its interphase functions but does not equivalently regulate all Ran-regulated SAFs in mitotic human cells.

RESULTS

NuMA Focuses Spindle Microtubules Using Its C-Terminal Conserved Microtubule-Binding Domain

NuMA has two microtubule-binding domains (MTBDs) at the C-terminal region^{33,37} (Figure 1B) that are critical for spindle-pole focusing.¹⁹ To understand which domain is required for spindle-pole focusing, we replaced endogenous NuMA with C-terminal truncation mutants (Figure 1B). Endogenous NuMA was fused with an mAID-mClover-FLAG (mACF) tag²⁰ (Figure S1A) and depleted using the AID system following doxycycline (Dox) and indole-3-acetic acid (IAA) treatment.^{20,36} In parallel, mCherry-tagged NuMA mutants were expressed from the Rosa 26 locus by Dox treatment (Figures 1B, 1C, S1B, and S1C).²⁰ Equivalent to endogenous NuMA, mCherry-tagged NuMA wild type (WT) accumulated in interphase nuclei (Figure S1C) and at mitotic spindle poles (Figure 1C) and was able to rescue pole-focusing defects caused by NuMA depletion (Figures 1C and 1D).²⁰ NuMA- Δ NLS mutants were unable to localize at nuclei in interphase (Figure S1C), but were able to accumulate at spindle poles to rescue pole-focusing defects (Figures 1C and 1D). As expected, NuMA Δ C-ter mutants, which lack both MTBDs, diffused into the cytoplasm during metaphase (Figure 1C) and were unable to rescue the spindle-pole focusing defects (Figures 1C and 1D).¹⁹ Similarly, NuMA Δ ex24 mutants, which lack the NLS and part of MTBD1, were unable to fully rescue focusing defects, despite localizing around the spindle poles (Figures 1C and 1D). Although this localization appears to be slightly reduced at the poles (Figure 1C), the fluorescence intensities were not significantly different between Δ ex24 and Δ NLS mutants at either mitotic poles or interphase cytoplasm (Figures S1D and S1E). In contrast, NuMA Δ (NLS+MTBD2) mutants, which accumulate on mitotic spindle poles and interphase microtubules around centrosomes, were able to rescue the focusing defects (Figures 1C, 1D, and S1C). These results indicate that NuMA's MTBD1, containing a well-conserved NuMA-Lin5-Mud (NLM) motif (Figure S1F),^{38,39} is essential for spindle-pole focusing in human cells, similar to mouse fibroblasts.²²

NuMA Localizes at the Spindle Poles Independently of RCC1

NuMA's MTBD1 is adjacent to the NLS, which is recognized by importin- α (Figures 1A, 1B, and S1F).³³ A recent *in vitro* study demonstrated that NuMA's microtubule-binding activity is sterically inhibited by the importin- α/β complex, but Ran-GTP releases the importin complex, allowing NuMA to interact with microtubules (Figure 1A).³³ To test this model in cells, we depleted RCC1 (RanGEF) by integrating an mAID-mClover (mAC) tag into the gene (Figures S1A and S2A; hereafter, all PCR validation results of the established cell lines are summarized in Figure S7).³⁶ Surprisingly, RCC1 depletion did not substantially affect NuMA's spindle-pole localization (Figure 2A). Although NuMA intensities at the spindle poles were

slightly reduced in RCC1-depleted cells (Figure 2B), the relative intensities of NuMA on microtubules slightly increased (Figure 2C) as a result of the reduction of microtubule intensities following RCC1 depletion (Figures 2A and S2B). RCC1 depletion also shortened the metaphase spindle (Figures 2A and 2D) and delayed mitotic progression (Figures S2C–S2E), but spindle poles were focused normally and the cells eventually exited mitosis, as reported in RCC1-depleted chicken DT40 cells.¹⁴ These results indicate that, although Ran-GTP is required for some aspects of spindle assembly, it is not required to localize and activate NuMA at the spindle poles in human cells.

NuMA Participates in Spindle-Pole Focusing Independently of RCC1

To further analyze the functions of NuMA in RCC1-depleted cells, we next co-depleted RCC1 and NuMA. Following treatment with Dox and IAA, both RCC1-mAC and NuMA-mAID-mCherry were depleted (Figure 2E), and unfocused spindles were frequently observed (Figures 2E and 2F). In addition, some spindles were completely collapsed and did not form a bi-polar spindle structure (Figures 2E, bottom, and 2F). Unexpectedly, co-depletion of RCC1 and NuMA further diminished the intensities of tubulin (Figures 2G and S2F). These results suggest that NuMA is functional in the absence of Ran-GTP to focus spindle poles and stabilize spindle microtubules.

We note that the frequency of an unfocused spindle in RCC1 and NuMA co-depleted cells (Figure 2F; ~20%) is lower than that of NuMA single-depleted cells (Figure 1D; ~74%). The milder phenotype might reflect smaller pole-splitting forces exerted in the co-depleted cells, as RCC1 depletion results in shorter metaphase spindle formation (Figure 2D) with reduced microtubules (Figure S2B).

RanGAP1 and Importin- β Degradation Do Not Affect NuMA Localization and Function at Spindle Poles

Although RCC1 is dispensable for NuMA localization and function, depletion of RanGAP1 or importin- β may cause overactivation of NuMA (Figure 1A), resulting in spindle assembly defects. To test this, we depleted either RanGAP1 or importin- β (Figures 2H–2K and S2G–S2J). RanGAP1 depletion did not affect NuMA's spindle-pole localization (Figures 2H and 2I), spindle length, or mitotic duration (Figure S2H). Importin- β depletion also did not affect NuMA's localization at spindle poles (Figures 2J and 2K), but it did result in short spindles and mitotic delay (Figure S2J).

To further test the contribution of the Ran-importin pathway to NuMA activation, we next expressed importin- α Δ IBB mutants that lack the importin- β -binding (IBB) domain (Figure S2K). Importin- α Δ IBB mutants are insensitive to Ran-GTP due to the lack of an IBB domain but are still able to interact with NuMA and partially inhibit NuMA's microtubule-binding activity *in vitro* (Figure S2K).³³ However, importin- α Δ IBB diffused into cytoplasm similarly to importin- α WT, and neither affected NuMA's spindle-pole localization or co-localized with NuMA at the spindle poles in our experimental conditions (Figures S2L and S2M). Together, these results indicate that the traditional Ran pathway (Figure 1A) is dispensable for NuMA regulation and activation in cultured human cells.

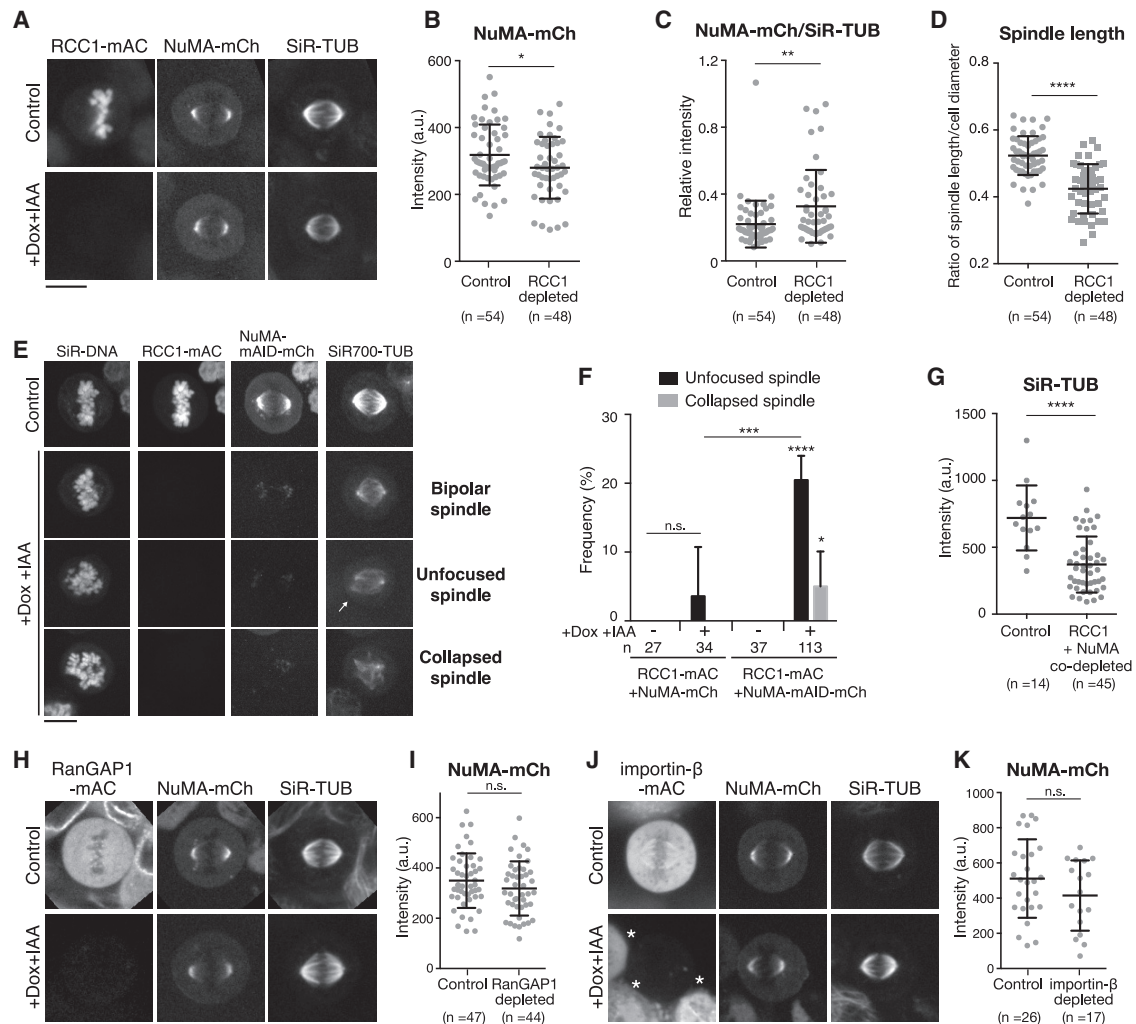


Figure 2. NuMA Functions in Spindle-Pole Focusing Independently of RCC1

(A) Live fluorescence images of metaphase RCC1-mAC cells 24 h after Dox and IAA treatment.
 (B) Intensity of NuMA-mCh at spindle poles in controls (318 ± 90.86) and RCC1-depleted cells (279.6 ± 92.39).
 (C) Relative intensity of NuMA-mCh/SiR-tubulin at spindle poles in controls (0.22 ± 0.14) and RCC1-depleted cells (0.33 ± 0.22).
 (D) Ratio of spindle length and cell diameter in controls and RCC1-depleted cells.
 (E) Live images of RCC1-mAC and NuMA-mAID-mCh double knockin cells 24 h after Dox and IAA treatment. Projected images from 5 z sections are shown. The arrow indicates unfocused microtubules.
 (F) Quantification of cells in (E) from >4 independent experiments. p values were calculated using Dunnett's multiple comparisons test after one-way ANOVA ($F(3,14) = 36.40$; $p = 0.0001$).
 (G) Intensity of SiR-tubulin at spindle poles in controls (719.6 ± 242.7) and RCC1 and NuMA co-depleted cells (371.1 ± 209.2).
 (H) Live images of metaphase RanGAP1-mAC cells 24 h after Dox and IAA treatment.
 (I) Quantification of NuMA-mCh signals at spindle poles in controls (349.6 ± 108.3) and RanGAP1-depleted cells (318.6 ± 107.7).
 (J) Live images of metaphase importin- β -mAC cells 24 h after Dox and IAA treatment. Asterisks indicate RCC1-non-depleted cells (see STAR Methods).
 (K) Quantification of NuMA-mCh signals at spindle poles in controls (511.2 ± 223) and importin- β -depleted cells (414.8 ± 199.5) from >3 independent experiments. See also Figure S2. Error bars indicate mean \pm SD; * $p < 0.05$, ** $p < 0.01$, *** $p < 0.001$, **** $p < 0.0001$; scale bars, 10 μ m.

Mitotic Degradation of RCC1 Does Not Affect Localization and Function of NuMA at Spindle Poles

In the above experiments, RCC1, RanGAP1, or importin- β were depleted in asynchronous culture. However, given Ran's function in interphase nuclear-cytoplasmic transport, unknown secondary effects may have induced their mitotic phenotypes. In addition, because NuMA is maintained in the nucleus following RCC1 depletion in interphase (Figure S2E; $t = -0:10$), the

majority of NuMA may already have been liberated from importins by pre-existing RCC1 and exist as an active form in the nucleus, thereby producing no aberrant phenotypes during mitosis. To exclude these possibilities, we next depleted RCC1 in nocodazole-arrested cells and analyzed the behavior of NuMA following nocodazole washout (Figure 3A).

In control cells, NuMA diffused into the cytoplasm during nocodazole arrest (Figure 3B; $t = -90$), but rapidly accumulated

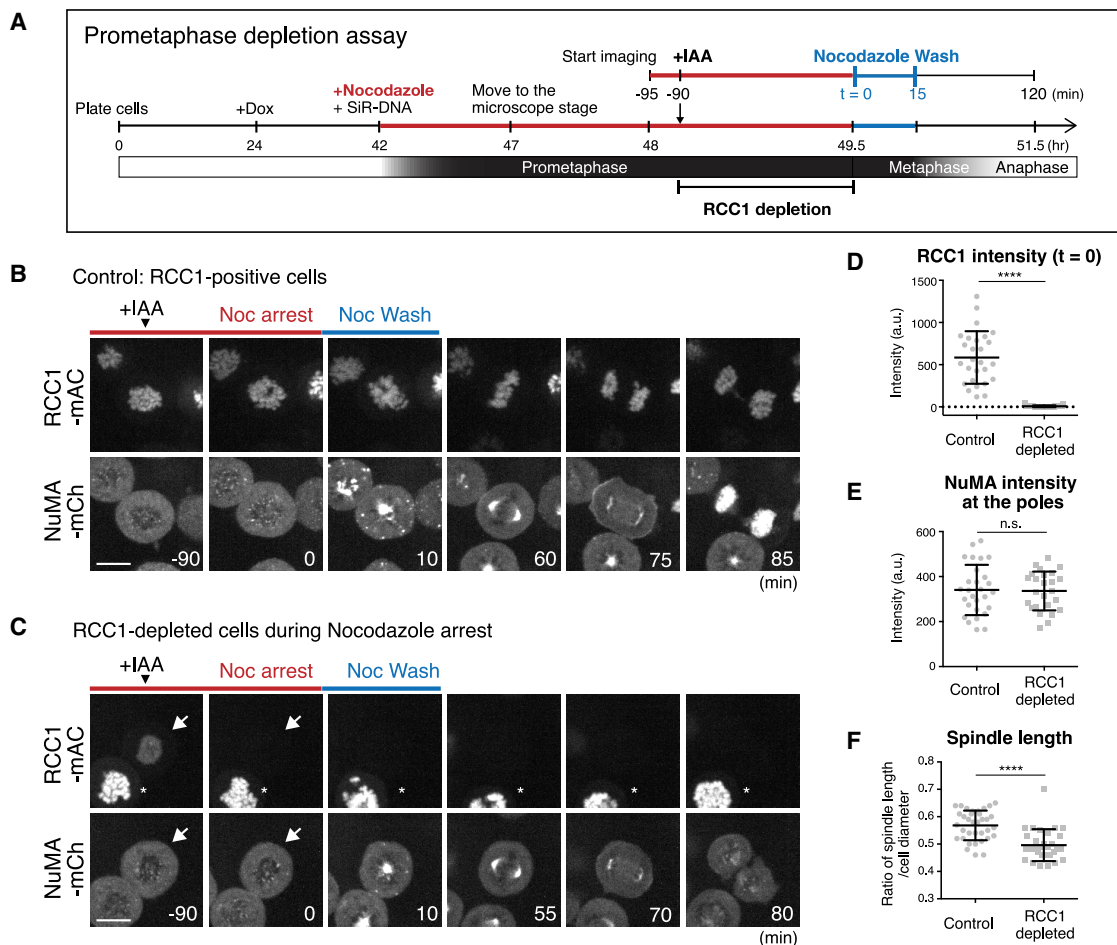


Figure 3. RCC1 Depletion during Prometaphase Does Not Affect NuMA Localization and Function at the Spindle Poles

(A) Diagram of prometaphase depletion assay (see STAR Methods).

(B and C) Live fluorescence images in RCC1-positive control (B) and RCC1-negative cells (C) treated with nocodazole and IAA, as described in (A). Arrows and asterisks indicate RCC1-depleted and non-depleted cells, respectively.

(D) Intensity of RCC1 on chromosomes at t = 0 in controls (585.2 ± 311.8 ; n = 27) and RCC1-depleted cells (7.6 ± 10.3 ; n = 25).

(E) Intensity of NuMA at metaphase spindle poles in controls (340.6 ± 111.6 ; n = 28) and RCC1-depleted cells (336.0 ± 86.5 ; n = 25). Welch's t test gave a p of 0.9542.

(F) Ratio of spindle length and cell diameter in control (0.57 ± 0.05 ; n = 35) and RCC1-depleted (0.50 ± 0.06 ; n = 30) cells from >3 independent experiments.

See also Figure S3 and Videos S1 and S2. Error bars indicate mean \pm SD; *p < 0.05, **p < 0.01, ***p < 0.001, ****p < 0.0001; scale bars, 10 μ m.

near chromosome masses following nocodazole washout (Figure 3B; t = 10; Video S1). Unexpectedly, NuMA also displayed punctate signals throughout cells (Figures 3B, t = 10, and S3A), some of which co-localized with SiR-tubulin (Figure 3B). These NuMA dots disappeared during spindle assembly, and the majority of NuMA localized at the poles of metaphase spindles within 60 min (Figure 3B; t = 60). Following mitotic exit, NuMA was localized in the nucleus (Figure 3B; t = 85).

Importantly, even if RCC1 was depleted during nocodazole arrest, NuMA accumulated as usual at focused spindle poles. RCC1-mAC signals were initially detectable (Figure 3C; t = -90, arrow), but were reduced to undetectable levels after addition of IAA (Figures 3C, t = 0, and 3D). After nocodazole-washout, NuMA accumulated near chromosome masses (Figure 3C; t = 10) and localized to focused spindle poles (Figure 3C; t = 55; Video S2), as observed in control cells (Figure 3E). During the

process, the number of NuMA dots appeared to be reduced (Figures 3C, t = 10, and S3C), but the number of SiR-tubulin dots on chromosomes, which might represent non-centrosomal microtubules nucleated from chromosomes, was not significantly affected by RCC1 depletion (Figure S3D). RCC1-depleted cells entered anaphase with timing similar to that of control cells (Figure S3E), but NuMA was absent from the nucleus after mitotic exit (Figure 3C; t = 80).

As observed when RCC1 was depleted in asynchronous culture (Figure 2D), the metaphase spindle became shorter when RCC1 was depleted during nocodazole arrest (Figure 3F). In addition, metaphase spindle poles were well focused, and unfocused NuMA signals were never observed in both control (n = 28) and RCC1-depleted (n = 25) cells. The frequency of mis-oriented spindles slightly increased in RCC1-depleted cells (Figure S3F), but the difference was not statistically significant. Taken together,

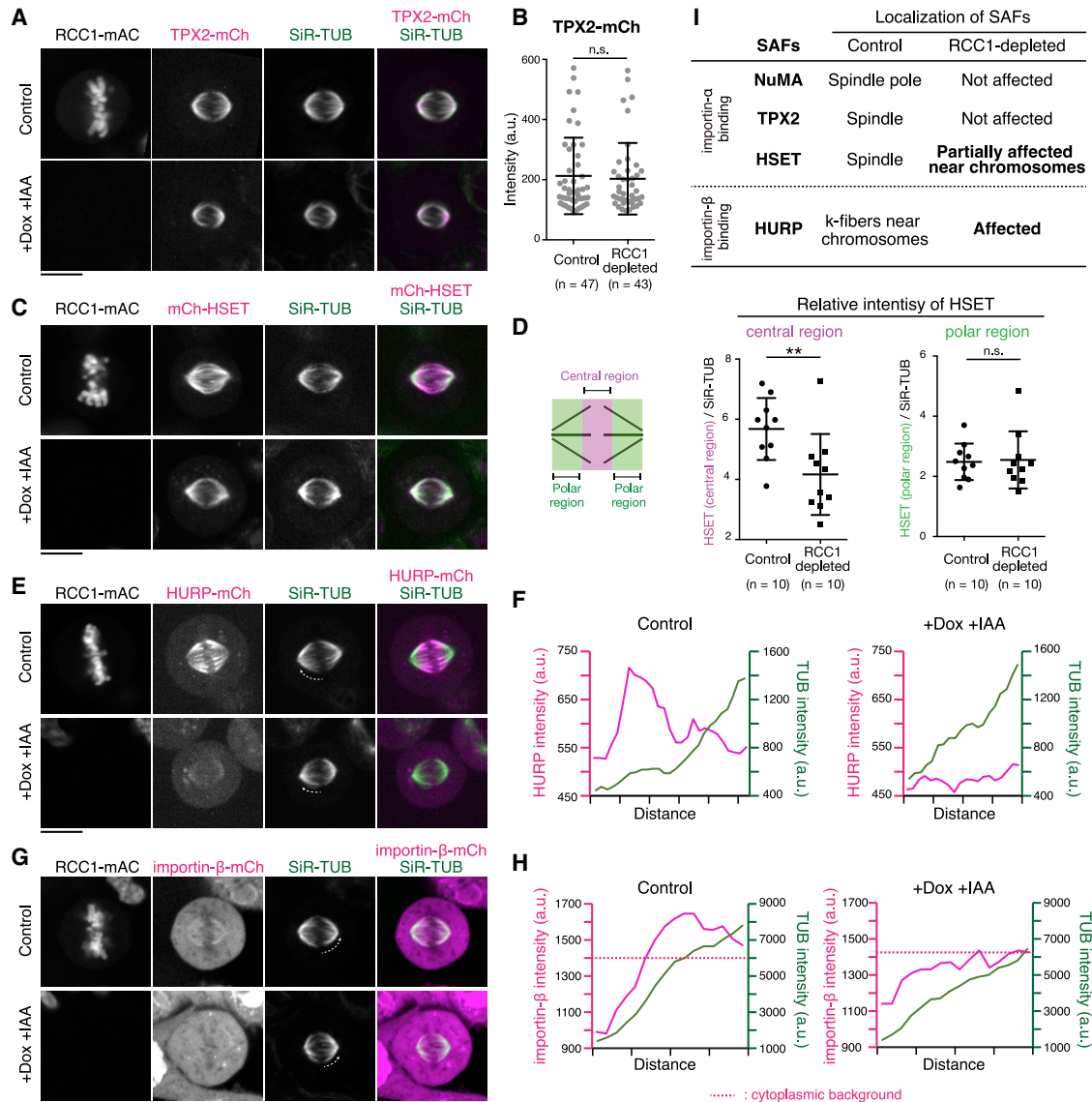


Figure 4. RCC1 Regulates Chromosome-Proximal Localization of HURP and HSET

(A, C, E, and G) Live fluorescent images of metaphase RCC1-mAC cells 24 h after Dox and IAA treatment.

(B) Intensity of TPX2-mCh at spindle poles in controls (212.7 ± 127.3) and RCC1-depleted cells (203.2 ± 119.1).

(D) Left: diagram showing the central and polar regions of the spindle. Right: relative intensity of mCh-HSET against SiR-tubulin at central regions in controls (5.68 ± 1.03) and RCC1-depleted cells (4.16 ± 1.34) and at polar regions in controls (2.48 ± 0.61) and RCC1-depleted cells (2.55 ± 0.95) is shown. Welch's t test gave a p of 0.67.

(F and H) Line scans showing fluorescence intensities of SiR-tubulin and HURP-mCh or importin-β-mCh on k-fibers indicated as dotted lines in (E) and (G), respectively.

(I) List summarizing localization of SAFs.

See also Figure S4. Error bars indicate mean \pm SD; *p < 0.05, **p < 0.01, ***p < 0.001, ****p < 0.0001; scale bars, 10 μ m.

these results indicate that RCC1 participates on some level in spindle assembly independently of its interphase functions, but is dispensable for NuMA localization and function at spindle poles.

RCC1 Regulates Chromosome-Proximal Localization of HURP and HSET

To elucidate Ran's spindle assembly function, we set out to identify SAFs regulated by Ran-GTP, initially focusing on the localization of 3 major SAFs: TPX2; HSET; and HURP. TPX2 co-localized

with SiR-tubulin signals in metaphase (Figure 4A, top), but its localization was virtually unaffected in RCC1-depleted cells (Figures 4A, bottom, and 4B). In contrast, HSET localized everywhere along spindle microtubules (Figure 4C, top),³¹ and following RCC1 depletion, its spindle localization was selectively reduced near chromosomes (Figures 4C, bottom, 4D, and S4A). Remarkably, HURP localization was affected by RCC1 depletion: HURP accumulated at kinetochore fibers (k-fibers) near chromosomes in all analyzed cells (n = 40), but

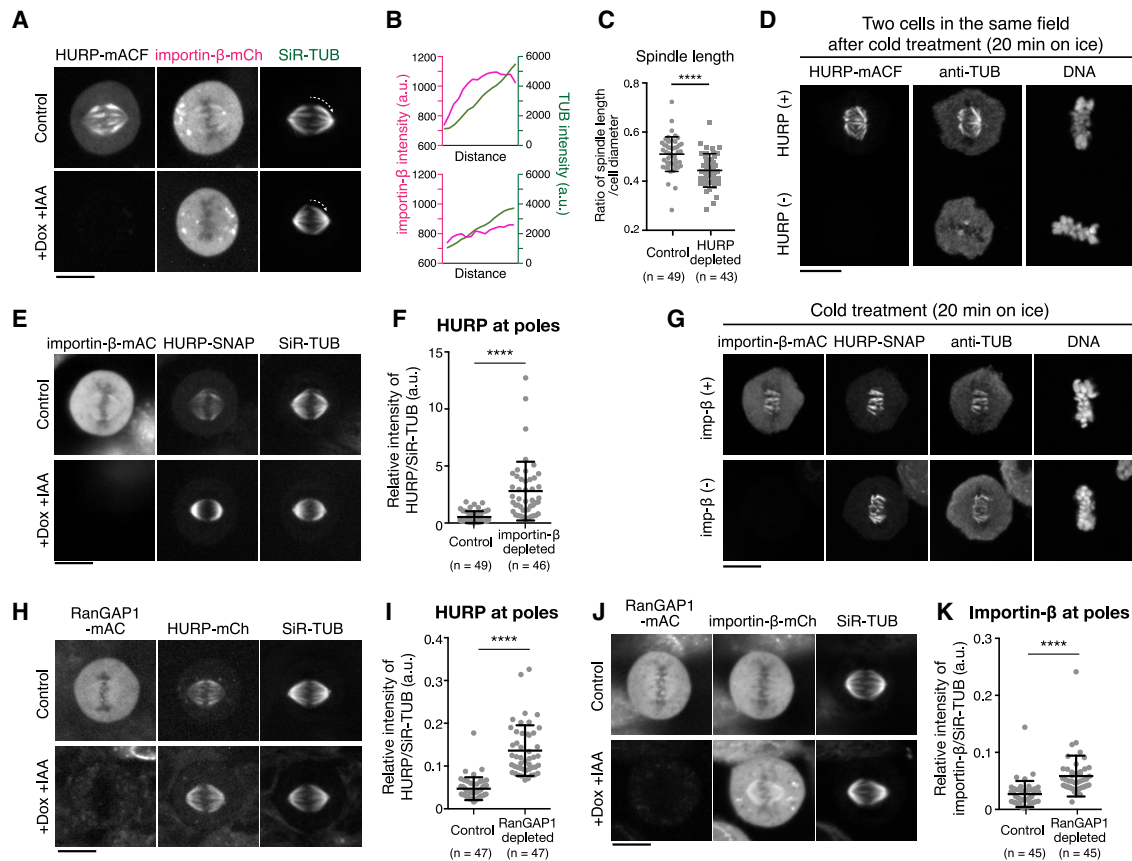


Figure 5. HURP, but Not Importin- β , Is Required to Stabilize K-Fibers

(A) Live fluorescence images of metaphase HURP-mACF (mAID-mClover-FLAG) cells 24 h after Dox and IAA treatment. (B) Line scans showing fluorescence intensities of SiR-tubulin and importin- β mCh on k-fibers indicated as dotted lines in (A). (C) Ratio of spindle length and cell diameter in control (0.64 ± 0.05) and HURP-depleted (0.52 ± 0.06) cells. (D) Fluorescence images of HURP-mACF, TUB, and DNA (Hoechst 33342) in metaphase fixed cells treated with ice-cold medium for 20 min. Two cells with or without HURP signals were analyzed in the same field. (E) Live images of metaphase importin- β -mACF cells 24 h after Dox and IAA treatment. (F) Relative intensities of HURP-mCh against SiR-tubulin at the poles in control (0.5217 ± 0.5171) and importin- β -depleted (2.802 ± 2.574) cells. (G) Fluorescence images of fixed metaphase cells treated with ice-cold medium for 20 min. Five z section images were obtained using 0.5- μ m spacing; maximum intensity projection images are shown in (D) and (G). (H and J) Live images of metaphase RanGAP1-mACF cells 24 h after Dox and IAA treatment. (I) Relative intensities of HURP-mCh against SiR-tubulin at the poles in control (0.04708 ± 0.02666) and RanGAP1-depleted (0.1362 ± 0.0592) cells. (K) Relative intensities of importin- β -mCh against SiR-tubulin at the poles in control (0.02695 ± 0.002289) and RanGAP1-depleted (0.05852 ± 0.03579) cells. See also Figure S5. Error bars indicate mean \pm SD; * $p < 0.05$, ** $p < 0.01$, *** $p < 0.001$, **** $p < 0.0001$; scale bars, 10 μ m.

localized weakly on spindle microtubules in all RCC1-depleted cells observed ($n = 43$; Figures 4E and 4F).

As we found that endogenous importin- β also accumulates at k-fibers in both living (Figures 2J and S4B) and fixed cells (Figure S4C), we next analyzed importin- β in RCC1-depleted cells. In 84% of control cells ($n = 45$), importin- β signals were detected in both k-fibers and cytoplasm (Figure 4G, top). However, the k-fiber signals were not detectable in 88% of RCC1-depleted cells ($n = 43$; Figure 4G, bottom). Although microtubule density is reduced to 60%–70% by RCC1 depletion (Figure S2B), the k-fiber signals of importin- β should still be detected, if they exist, as cytoplasmic intensities of importin- β were not significantly changed by RCC1 depletion (Figures 4H and S4D).

Together, these results suggest that the Ran-GTP gradient activates at least two established SAFs, HSET and HURP,

preferentially near chromosomes, but does not affect NuMA and TPX2 (Figure 4I).

HURP, but Not Importin- β , Is Required to Stabilize K-Fibers

Importin- β acts as an inhibitor of HURP (Figure 1A).³² However, importin- β co-localizes with HURP at k-fibers (Figure S4C) and behaves similarly to HURP downstream of Ran-GTP (Figures 4E and 4G). To understand the relationship between HURP and importin- β , we next sought to deplete endogenous HURP using AID (Figures 5A and S5A). Importin- β was detected on k-fibers in 81% of control cells ($n = 49$; Figures 5A and 5B), but not observed in any HURP-depleted cells analyzed ($n = 43$; Figures 5A and 5B). HURP depletion also reduced mitotic spindle length (Figure 5C), but it did not significantly change microtubule

density at the poles (Figure S5B). Consistent with a previous study,³² HURP localized to cold-stable microtubules (Figure 5D, top), which were subsequently disrupted by HURP depletion (Figure 4D, bottom).

We next depleted importin- β (Figure 5E). Importin- β depletion caused a remarkable re-localization of HURP from k-fibers to spindle microtubules (Figures 5E and 5F). Although k-fiber localization of HURP was unclear in importin- β -depleted cells due to the relatively strong accumulation of HURP on spindle microtubules around spindle poles (Figure 5E, bottom), HURP was clearly detected on cold-stable k-fibers in importin- β -depleted cells (Figure 5G, bottom). These results suggest that HURP acts in k-fiber stabilization independently of importin- β .

HURP and Importin- β Localize throughout the Spindle in RanGAP1-Depleted Cells

To better understand the mechanisms of Ran-based spatial regulation of HURP and importin- β , we next analyzed the behavior of HURP and importin- β in RanGAP1-depleted cells, in which Ran-GTP should exist evenly throughout the cell. Interestingly, both HURP and importin- β localized throughout the spindle with increased intensities in RanGAP1-depleted cells (Figures 5H–5K). These results suggest that HURP and importin- β act together and interact with microtubules preferentially in the presence of Ran-GTP.

Fast Turnover of Chromosome-Proximal HURP in the Presence of Importin- β

Based on our results, we developed a local cycling model for the activation and polarization of HURP (Figure S5C). In this model, importin- β inhibits HURP globally, including at k-fibers, by masking HURP's 2nd microtubule-binding domain (MTBD2).⁴⁰ The resulting HURP-importin- β complex binds weakly to microtubules through HURP's MTBD1,⁴⁰ but the Ran-GTP gradient locally releases importin- β from HURP, resulting in the full activation of HURP near chromosomes (Figure S5C). To test this model, we performed fluorescence recovery after photobleaching (FRAP) for HURP and analyzed its dynamics on spindle microtubules in the presence and absence of importin- β . In control cells, HURP quickly recovered at k-fibers near chromosomes after bleaching (Figures 6A, top, 6B, left, black, and S6A; $t_{1/2} = 20.5$ s). In contrast, HURP's recovery was hardly seen on the spindle in importin- β -depleted cells (Figures 6A, bottom, 6B, red, and S6B), suggesting a stable binding to spindle microtubules.

HURP Is Dynamically Maintained at K-Fibers during Metaphase

To confirm the dynamic regulation of HURP by importin- β and Ran-GTP, we next sought to deplete importin- β during metaphase (Figure 6C).⁴¹ Following treatment with the antigen-presenting cell (APC)/C inhibitors, apcin and proTAME, cells were arrested at metaphase, at which point both importin- β and HURP accumulated at k-fibers near chromosomes (Figure 6D; $t = 0$). Importantly, importin- β -mAC signals diminished to undetectable levels 60–90 min after the addition of IAA (Figure 6D, arrows), and HURP relocated from k-fibers to spindle

microtubules in response to the reduction of importin- β (Figures 6D and 6E).

To confirm these results, we next acutely depleted RCC1 in metaphase-arrested cells. As with importin- β depletion, HURP dissociated from k-fibers and localized weakly on the spindle in response to RCC1 depletion (Figures 7A and 7B; Video S3). However, in contrast to the prometaphase depletion assay (Figure 3F), spindle length appeared to be normal when RCC1 was depleted in the metaphase-arrested condition (Figure 7C). In addition, SiR-tubulin intensities at the poles did not significantly change when RCC1 was depleted during metaphase (Figure 7D). To compare these phenotypes, we lastly depleted HURP via auxin, which significantly reduced HURP signals 90–120 min following treatment (Figures 7E and 7F). In contrast to RCC1 depletion, the metaphase spindle became shorter in response to the depletion of HURP (Figures 7E and 7G).

Taken together, these results indicate that HURP is dynamically maintained at k-fibers near chromosomes by the Ran-importin pathway, even in metaphase. In addition, HURP is required to maintain spindle length during metaphase (Figure 7G), whereas Ran-GTP appears to contribute to spindle length control preferentially during prometaphase (Figures 3F and 7C).

DISCUSSION

NuMA Is Liberated from Importins Independently of Ran-GTP for Spindle-Pole Focusing

In contrast to the prevailing model (Figure 1A), we demonstrated that the Ran-Importin pathway is dispensable for localization and function of NuMA at spindle poles in human HCT116 cells (Figures 2 and 3). This is consistent with the recent observation that NuMA is less sensitive to Ran-GTP levels than to HSET/XCTK2.³⁰ Although we do not exclude the possibility that Ran-GTP liberates NuMA from importin- α/β complexes near chromosomes, we favor the idea that parallel pathways exist to activate NuMA in mitotic human cells (Figure 7H). In fact, recent studies indicate that importin- α/β -binding TPX2 can be activated not only by Ran-GTP but also by Golgi- or palmitoylation-dependent sequestration of importin- α .^{42,43} In addition, phosphorylation of TPX2's NLS also acts to release importins from TPX2.⁴⁴ Similar mechanisms might exist for NuMA around centrosomes (Figure 7H).

Although TPX2-NLS is well conserved in vertebrates, the NLS of NuMA is not well conserved in fish (Figure S1F). Furthermore, the NLS is absent in other NuMA-like proteins in lower eukaryotes.^{38,45,46} Future research should be undertaken to understand how the NuMA-importin interaction is regulated in a Ran-independent manner and why NLS-dependent regulation of NuMA was acquired in higher animals.

The Ran-Importin Pathway Locally Activates HURP by Promoting Its Microtubule Binding-Dissociation Cycle Near Chromosomes

In contrast to NuMA, we demonstrated that HURP is preferentially regulated by the Ran-importin pathway in mitotic human cells (Figures 4E, 5H, and 5J). Although HURP has been identified previously as a downstream target of Ran-GTP,³² we found that HURP also co-localizes with importin- β on k-fibers near

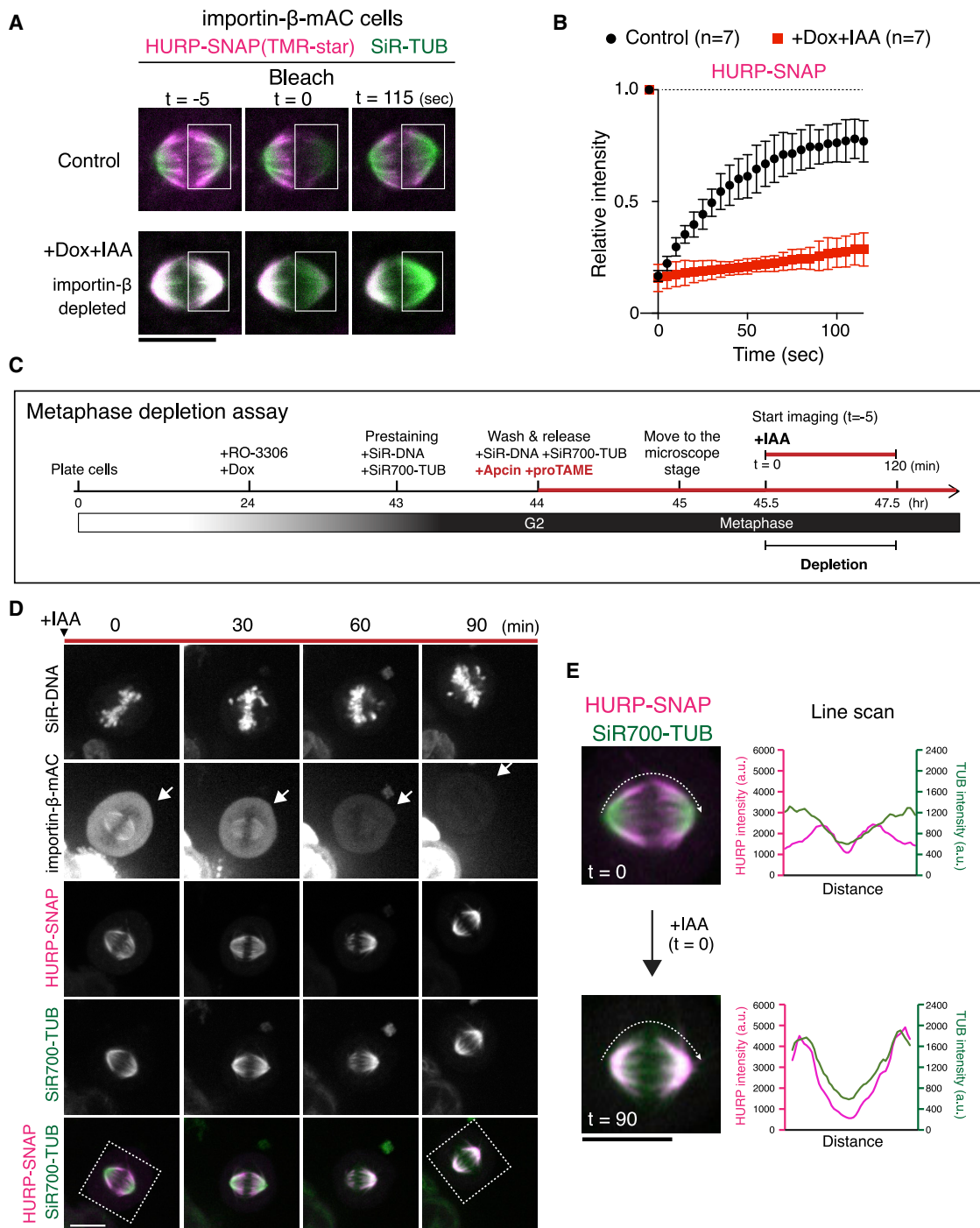


Figure 6. HURP Dynamically Accumulates on Metaphase K-Fibers in an Importin- β -Dependent Manner

(A) Live fluorescence images of HURP-SNAP visualized with TMR-star and SiR-tubulin in control and importin- β -depleted cells. Fluorescence signals were bleached in the boxed regions at $t = 0$, and fluorescence recovery was monitored for 120 s.

(B) FRAP plots of means with SDs from 7 samples.

(C) Diagram of metaphase depletion assay (see STAR Methods).

(D) Live images of DNA, tubulin, and indicated proteins. IAA was added at $t = 0$. Arrows indicate a cell showing a reduction of importin- β during metaphase.

(E) Enlarged images from (D) and line scans of HURP and SiR-tubulin intensities on spindle microtubules indicated as dotted lines in the left images, showing a re-localization of HURP from k-fibers ($t = 0$) to the spindle ($t = 90$).

See also Figure S6. Error bars indicate mean \pm SD; scale bars, 10 μ m.

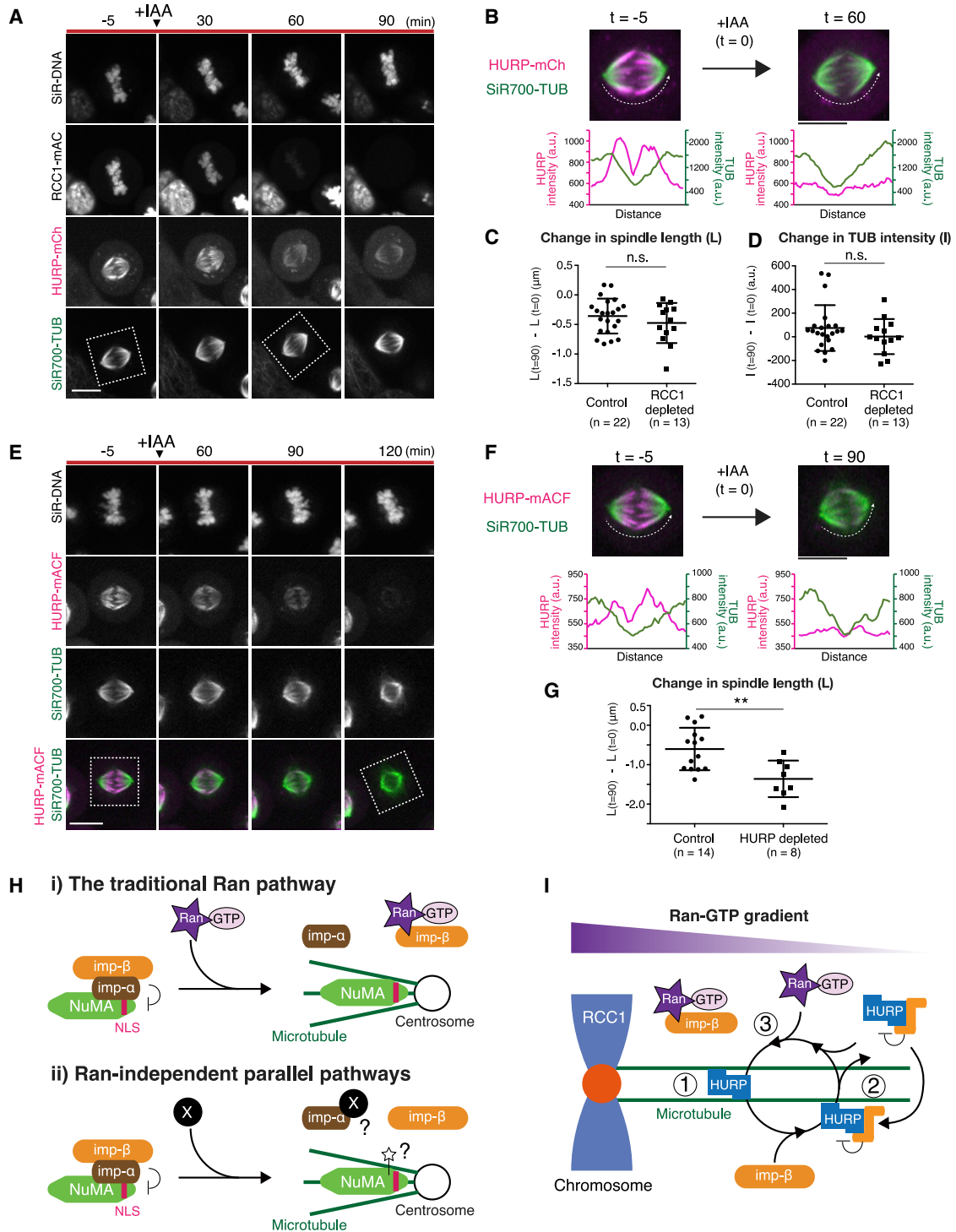


Figure 7. Models of Local Activation Mechanisms for HURP and NuMA in Mitosis

(A) Live fluorescence images of DNA, tubulin, and indicated proteins. IAA was added at $t = 0$.

(B) Enlarged images of indicated regions in (A) and line scans of indicated microtubules, showing a reduction of HURP-mCh from k-fibers in response to RCC1 depletion.

(C) Change in spindle length in control (-0.36 ± 0.30) and RCC1-depleted (-0.47 ± 0.34) cells.

(D) Change in SiR-tubulin intensities in control (74.2 ± 193.4) and RCC1-depleted (2.269 ± 148.1) cells. Welch's t test gave a p of 0.505 in (C) and 0.275 in (D).

(E) Live images of indicated proteins. IAA was added at $t = 0$.

(F) Enlarged images of indicated regions in (E) and line scans of indicated microtubules, showing a reduction of HURP-mACF.

(G) Change in SiR-tubulin intensities in control (-0.60 ± 0.54) and RCC1-depleted (-1.36 ± 0.46) cells from >3 independent experiments.

(legend continued on next page)

chromosomes (Figures S4C, 5A, and 5E) and stabilizes k-fibers independently of importin- β (Figures 5D and 5G). Based on these and other results (Figures 4E, 5E, 5H, 6A, 6D, and 7A), we propose a local cycling model for the establishment and maintenance of HURP's polarized localization to spindle microtubules (Figures 7I and S5C). This model nicely explains the reason why HURP, but not importin- β , stabilizes microtubules and generates stable k-fibers near chromosomes (Figures 5D and 5G). This dynamic regulation is similar to that of HSET/XCTK2⁴⁷ and would be suitable for bundling short microtubules around kinetochores during prometaphase⁴⁸ and for coupling HURP's polarized localization with microtubule flux on the metaphase spindle.

RCC1 Promotes Proper Spindle Assembly in Human Mitotic Cells

By depleting RCC1 during prometaphase, we demonstrated that RCC1 participates in proper spindle assembly independently of its interphase function in human mitotic cells (Figure 3F). Short spindles caused by RCC1 depletion could be explained by multiple defects, including the lack of HURP-based k-fiber formation (Figures 5C and 5D) and HSET-dependent spindle elongation (Figure 4C).³¹ Although HURP depletion shortened the metaphase spindle (Figure 7E), RCC1 depletion in metaphase did not affect spindle length (Figure 7A). The HURP-importin- β complex may therefore play a role in the maintenance of the established spindle structure in RCC1-depleted cells.

In addition to spindle assembly, Ran-GTP also contributes to microtubule nucleation during mitosis.²⁸ Microtubule intensities were reduced when RCC1 was depleted before mitosis (Figures 2A and S2B), but not during metaphase (Figures 7A and 7D). Once microtubule nucleation pathways are activated in mitosis, additional Ran-based activation may not be required. Alternatively, the requirement of Ran for microtubule nucleation may be different between cell types. Unexpectedly, we found that NuMA's punctate signals appear transiently in a Ran-GTP-dependent manner (Figures 3B, 3C, and S3C). The significance of the NuMA puncta is currently unclear, but these may be related to minus-end stabilization of nucleated microtubules.

A New Toolkit and Mitosis-Specific Protein-Depletion Assays to Dissect the Mitotic Roles of the Ran-Importin Pathway

Mitotic inactivation is critical to precisely analyze mitotic functions of the Ran pathway. Previously, tsBN2, a temperature-sensitive RCC1 mutant hamster cell line,^{49,50} and a small-molecule inhibitor, importazole,⁵¹ have been developed to acutely inhibit functions of RCC1 and importin- β , respectively. Here, we established many human AID-cell lines (Table S1)³⁶ and succeeded in depleting RCC1 specifically in prometaphase (Figures 3A–3C) or metaphase (Figures 7A and 7E). As these AID cell lines and mitotic depletion assays are applicable to

other Ran-regulated proteins^{4,50,52} and other multi-functional proteins, such as dynein and NuMA,^{20,36} they can be used to further advance our understanding of the mechanisms and roles of spindle assembly, maintenance, and positioning in animal cells.

STAR★METHODS

Detailed methods are provided in the online version of this paper and include the following:

- KEY RESOURCES TABLE
- RESOURCE AVAILABILITY
 - Lead Contact
 - Materials Availability
 - Data and Code Availability
- EXPERIMENTAL MODEL AND SUBJECT DETAILS
- METHOD DETAILS
 - Plasmid Construction
 - Cell Culture, Cell Line Generation, and Antibodies
 - Microscope System
 - Immunofluorescence and Live Cell Imaging
 - Prometaphase Depletion Assay and Nocodazole Washout
 - Metaphase Depletion Assay
 - Cold Treatment Assay
 - FRAP
- QUANTIFICATION AND STATISTICAL ANALYSIS
 - Quantification of Fluorescent Intensities
 - Statistical Analysis

SUPPLEMENTAL INFORMATION

Supplemental Information can be found online at <https://doi.org/10.1016/j.cub.2020.09.091>.

ACKNOWLEDGMENTS

We thank Iain M. Cheeseman for critical reading of the manuscript and Yuki Tsukada, Rie Inaba, Kiyoko Murase, Taisei Kumazaki, and Susan Boerner for technical assistance. This work was supported by grants from the PRESTO program (JPMJPR13A3) of the Japan Science and Technology Agency (JST) to T.K.; a Career Development Award of the Human Frontier Science Program (CDA00057/2014-C) to T.K.; KAKENHI (16K14721 and 17H05002 to T.K. and 17H01431 for G.G. and T.K.) of the Japan Society for the Promotion of Science (JSPS); NIG-JOINT (2014B-B-3, 2015-A1-19, and 2016-A1-22 to T.K.) of National Institute of Genetics (NIG); the Naito Foundation to T.K.; and JSPS and DFG (Deutsche Forschungsgemeinschaft, Germany) under the Joint Research Projects-LEAD with UKRI (UK Research and Innovation, UK) to G.G.

AUTHOR CONTRIBUTIONS

Conceptualization, T.K.; Investigation, T.K., K.T., H.H., M.N., and M.O.; Formal Analysis, T.K. and K.T.; Methodology, T.K., Y.S., and M.T.K.; Writing, T.K.; Supervision, T.K. and G.G.; Funding Acquisition, T.K. and G.G.

(H) Models of the traditional Ran pathway (i) and Ran-independent parallel pathway (ii). The Ran-independent parallel pathway would activate NuMA away from chromosomes.

(I) A local cycling model of HURP on k-fibers. HURP strongly interacts with microtubules through its two MTBDs (1). Importin- β reduces HURP's microtubule-binding affinity by masking one of HURP's MTBDs (2). However, in the vicinity of chromosomes, Ran-GTP releases HURP from importin- β , resulting in local activation of HURP (3).

See also Video S3. Error bars indicate mean \pm SD; * p < 0.05, ** p < 0.01, *** p < 0.001, **** p < 0.0001; scale bars, 10 μ m.

DECLARATION OF INTERESTS

The authors declare no competing interests.

Received: April 24, 2020

Revised: August 25, 2020

Accepted: September 30, 2020

Published: November 12, 2020

REFERENCES

- Reber, S., and Hyman, A.A. (2015). Emergent properties of the metaphase spindle. *Cold Spring Harb. Perspect. Biol.* *7*, a015784.
- Heald, R., and Khodjakov, A. (2015). Thirty years of search and capture: the complex simplicity of mitotic spindle assembly. *J. Cell Biol.* *211*, 1103–1111.
- Kalab, P., and Heald, R. (2008). The RanGTP gradient - a GPS for the mitotic spindle. *J. Cell Sci.* *121*, 1577–1586.
- Forbes, D.J., Travesa, A., Nord, M.S., and Bernis, C. (2015). Reprint of "Nuclear transport factors: global regulation of mitosis". *Curr. Opin. Cell Biol.* *34*, 122–134.
- Bischoff, F.R., and Ponstingl, H. (1991). Catalysis of guanine nucleotide exchange on Ran by the mitotic regulator RCC1. *Nature* *354*, 80–82.
- Bischoff, F.R., Klebe, C., Kretschmer, J., Wittinghofer, A., and Ponstingl, H. (1994). RanGAP1 induces GTPase activity of nuclear Ras-related Ran. *Proc. Natl. Acad. Sci. USA* *91*, 2587–2591.
- Kalab, P., Weis, K., and Heald, R. (2002). Visualization of a Ran-GTP gradient in interphase and mitotic *Xenopus* egg extracts. *Science* *295*, 2452–2456.
- Kaláb, P., Pralle, A., Isacoff, E.Y., Heald, R., and Weis, K. (2006). Analysis of a RanGTP-regulated gradient in mitotic somatic cells. *Nature* *440*, 697–701.
- Dumont, J., Petri, S., Pellegrin, F., Terret, M.E., Bohnsack, M.T., Rassinier, P., Georget, V., Kalab, P., Gruss, O.J., and Verlhac, M.H. (2007). A centriole- and RanGTP-independent spindle assembly pathway in meiosis I of vertebrate oocytes. *J. Cell Biol.* *176*, 295–305.
- Moutinho-Pereira, S., Stuurman, N., Afonso, O., Hornsveld, M., Aguiar, P., Goshima, G., Vale, R.D., and Maiato, H. (2013). Genes involved in centrosome-independent mitotic spindle assembly in *Drosophila* S2 cells. *Proc. Natl. Acad. Sci. USA* *110*, 19808–19813.
- Hasegawa, K., Ryu, S.J., and Kaláb, P. (2013). Chromosomal gain promotes formation of a steep RanGTP gradient that drives mitosis in aneuploid cells. *J. Cell Biol.* *200*, 151–161.
- Holubcová, Z., Blayney, M., Elder, K., and Schuh, M. (2015). Human oocytes. Error-prone chromosome-mediated spindle assembly favors chromosome segregation defects in human oocytes. *Science* *348*, 1143–1147.
- Drutovic, D., Duan, X., Li, R., Kalab, P., and Solc, P. (2020). RanGTP and importin β regulate meiosis I spindle assembly and function in mouse oocytes. *EMBO J.* *39*, e101689.
- Furuta, M., Hori, T., and Fukagawa, T. (2016). Chromatin binding of RCC1 during mitosis is important for its nuclear localization in interphase. *Mol. Biol. Cell* *27*, 371–381.
- Nachury, M.V., Maresca, T.J., Salmon, W.C., Waterman-Storer, C.M., Heald, R., and Weis, K. (2001). Importin beta is a mitotic target of the small GTPase Ran in spindle assembly. *Cell* *104*, 95–106.
- Wiese, C., Wilde, A., Moore, M.S., Adam, S.A., Merdes, A., and Zheng, Y. (2001). Role of importin-beta in coupling Ran to downstream targets in microtubule assembly. *Science* *291*, 653–656.
- Gruss, O.J., Carazo-Salas, R.E., Schatz, C.A., Guarguaglini, G., Kast, J., Wilm, M., Le Bot, N., Vernos, I., Karsenti, E., and Mattaj, J.W. (2001). Ran induces spindle assembly by reversing the inhibitory effect of importin alpha on TPX2 activity. *Cell* *104*, 83–93.
- Stewart, M. (2007). Molecular mechanism of the nuclear protein import cycle. *Nat. Rev. Mol. Cell Biol.* *8*, 195–208.
- Hueschen, C.L., Kenny, S.J., Xu, K., and Dumont, S. (2017). NuMA recruits dynein activity to microtubule minus-ends at mitosis. *eLife* *6*, e29328.
- Okumura, M., Natsume, T., Kanemaki, M.T., and Kiyomitsu, T. (2018). Dynein-dynactin-NuMA clusters generate cortical spindle-pulling forces as a multi-arm ensemble. *eLife* *7*, e36559.
- Gaglio, T., Saredi, A., and Compton, D.A. (1995). NuMA is required for the organization of microtubules into aster-like mitotic arrays. *J. Cell Biol.* *131*, 693–708.
- Silk, A.D., Holland, A.J., and Cleveland, D.W. (2009). Requirements for NuMA in maintenance and establishment of mammalian spindle poles. *J. Cell Biol.* *184*, 677–690.
- Wittmann, T., Wilm, M., Karsenti, E., and Vernos, I. (2000). TPX2, a novel *Xenopus* MAP involved in spindle pole organization. *J. Cell Biol.* *149*, 1405–1418.
- Garrett, S., Auer, K., Compton, D.A., and Kapoor, T.M. (2002). hTPX2 is required for normal spindle morphology and centrosome integrity during vertebrate cell division. *Curr. Biol.* *12*, 2055–2059.
- Petry, S., Groen, A.C., Ishihara, K., Mitchison, T.J., and Vale, R.D. (2013). Branching microtubule nucleation in *Xenopus* egg extracts mediated by augmin and TPX2. *Cell* *152*, 768–777.
- Roostalu, J., Cade, N.I., and Surrey, T. (2015). Complementary activities of TPX2 and chTOG constitute an efficient importin-regulated microtubule nucleation module. *Nat. Cell Biol.* *17*, 1422–1434.
- King, M.R., and Petry, S. (2020). Phase separation of TPX2 enhances and spatially coordinates microtubule nucleation. *Nat. Commun.* *11*, 270.
- Scrofani, J., Sardon, T., Meunier, S., and Vernos, I. (2015). Microtubule nucleation in mitosis by a RanGTP-dependent protein complex. *Curr. Biol.* *25*, 131–140.
- Ems-McClung, S.C., Zheng, Y., and Walczak, C.E. (2004). Importin alpha/beta and Ran-GTP regulate XCTK2 microtubule binding through a bipartite nuclear localization signal. *Mol. Biol. Cell* *15*, 46–57.
- Ems-McClung, S.C., Emch, M., Zhang, S., Mahnoor, S., Weaver, L.N., and Walczak, C.E. (2020). RanGTP induces an effector gradient of XCTK2 and importin α/β for spindle microtubule cross-linking. *J. Cell Biol.* *219*, e201906045.
- Cai, S., Weaver, L.N., Ems-McClung, S.C., and Walczak, C.E. (2009). Kinesin-14 family proteins HSET/XCTK2 control spindle length by cross-linking and sliding microtubules. *Mol. Biol. Cell* *20*, 1348–1359.
- Silljé, H.H., Nagel, S., Körner, R., and Nigg, E.A. (2006). HURP is a Ran-importin beta-regulated protein that stabilizes kinetochore microtubules in the vicinity of chromosomes. *Curr. Biol.* *16*, 731–742.
- Chang, C.C., Huang, T.L., Shimamoto, Y., Tsai, S.Y., and Hsia, K.C. (2017). Regulation of mitotic spindle assembly factor NuMA by importin- β . *J. Cell Biol.* *216*, 3453–3462.
- Giesecke, A., and Stewart, M. (2010). Novel binding of the mitotic regulator TPX2 (target protein for *Xenopus* kinesin-like protein 2) to importin- α . *J. Biol. Chem.* *285*, 17628–17635.
- Kiyomitsu, T. (2019). The cortical force-generating machinery: how cortical spindle-pulling forces are generated. *Curr. Opin. Cell Biol.* *60*, 1–8.
- Natsume, T., Kiyomitsu, T., Saga, Y., and Kanemaki, M.T. (2016). Rapid protein depletion in human cells by auxin-inducible degron tagging with short homology donors. *Cell Rep.* *15*, 210–218.
- Gallini, S., Carminati, M., De Mattia, F., Pirovano, L., Martini, E., Oldani, A., Asteriti, I.A., Guarguaglini, G., and Mapelli, M. (2016). NuMA phosphorylation by Aurora-A orchestrates spindle orientation. *Curr. Biol.* *26*, 458–469.
- Siller, K.H., Cabernard, C., and Doe, C.Q. (2006). The NuMA-related Mud protein binds Pins and regulates spindle orientation in *Drosophila* neuroblasts. *Nat. Cell Biol.* *8*, 594–600.
- Du, Q., Stukenberg, P.T., and Macara, I.G. (2001). A mammalian Partner of inscuteable binds NuMA and regulates mitotic spindle organization. *Nat. Cell Biol.* *3*, 1069–1075.
- Song, L., Craney, A., and Rape, M. (2014). Microtubule-dependent regulation of mitotic protein degradation. *Mol. Cell* *53*, 179–192.

41. Sackton, K.L., Dimova, N., Zeng, X., Tian, W., Zhang, M., Sackton, T.B., Meaders, J., Pfaff, K.L., Sigoiilot, F., Yu, H., et al. (2014). Synergistic blockade of mitotic exit by two chemical inhibitors of the APC/C. *Nature* *514*, 646–649.
42. Wei, J.H., Zhang, Z.C., Wynn, R.M., and Seemann, J. (2015). GM130 regulates Golgi-derived spindle assembly by activating TPX2 and capturing microtubules. *Cell* *162*, 287–299.
43. Brownlee, C., and Heald, R. (2019). Importin α partitioning to the plasma membrane regulates intracellular scaling. *Cell* *176*, 805–815.e8.
44. Eibes, S., Gallisà-Suñe, N., Rosas-Salvans, M., Martínez-Delgado, P., Vernos, I., and Roig, J. (2018). Nek9 phosphorylation defines a new role for TPX2 in Eg5-dependent centrosome separation before nuclear envelope breakdown. *Curr. Biol.* *28*, 121–129.e4.
45. Lorson, M.A., Horvitz, H.R., and van den Heuvel, S. (2000). LIN-5 is a novel component of the spindle apparatus required for chromosome segregation and cleavage plane specification in *Caenorhabditis elegans*. *J. Cell Biol.* *148*, 73–86.
46. Greenberg, S.R., Tan, W., and Lee, W.L. (2018). Num1 versus NuMA: insights from two functionally homologous proteins. *Biophys. Rev.* *10*, 1631–1636.
47. Weaver, L.N., Ems-McClung, S.C., Chen, S.H., Yang, G., Shaw, S.L., and Walczak, C.E. (2015). The Ran-GTP gradient spatially regulates XCTK2 in the spindle. *Curr. Biol.* *25*, 1509–1514.
48. Sikirzhyski, V., Renda, F., Tikhonenko, I., Magidson, V., McEwen, B.F., and Khodjakov, A. (2018). Microtubules assemble near most kinetochores during early prometaphase in human cells. *J. Cell Biol.* *217*, 2647–2659.
49. Nishimoto, T., Eilen, E., and Basilico, C. (1978). Premature of chromosome condensation in a ts DNA- mutant of BHK cells. *Cell* *15*, 475–483.
50. Kiyomitsu, T., and Cheeseman, I.M. (2012). Chromosome- and spindle-pole-derived signals generate an intrinsic code for spindle position and orientation. *Nat. Cell Biol.* *14*, 311–317.
51. Soderholm, J.F., Bird, S.L., Kalab, P., Sampathkumar, Y., Hasegawa, K., Uehara-Bingen, M., Weis, K., and Heald, R. (2011). Importazole, a small molecule inhibitor of the transport receptor importin- β . *ACS Chem. Biol.* *6*, 700–708.
52. Kiyomitsu, T., and Cheeseman, I.M. (2013). Cortical dynein and asymmetric membrane elongation coordinately position the spindle in anaphase. *Cell* *154*, 391–402.
53. Schindelin, J., Arganda-Carreras, I., Frise, E., Kaynig, V., Longair, M., Pietzsch, T., Preibisch, S., Rueden, C., Saalfeld, S., Schmid, B., et al. (2012). Fiji: an open-source platform for biological-image analysis. *Nat. Methods* *9*, 676–682.
54. Kiyomitsu, T., Murakami, H., and Yanagida, M. (2011). Protein interaction domain mapping of human kinetochore protein Blinkin reveals a consensus motif for binding of spindle assembly checkpoint proteins Bub1 and BubR1. *Mol. Cell. Biol.* *31*, 998–1011.
55. Goshima, G., Nédélec, F., and Vale, R.D. (2005). Mechanisms for focusing mitotic spindle poles by minus end-directed motor proteins. *J. Cell Biol.* *171*, 229–240.

STAR★METHODS

KEY RESOURCES TABLE

REAGENT or RESOURCE	SOURCE	IDENTIFIER
Chemicals		
SiR-tubulin	Spirochrome	Cat# SC002
SiR-DNA	Spirochrome	Cat# SC007
SiR700-tubulin	Spirochrome	Cat# SC014
SNAP Cell 647-SiR	New England BioLabs	Cat# S9102S
SNAP Cell TMR-star	New England BioLabs	Cat# S9105S
Hoechst 33342	Sigma-Aldrich	Cat# B2261
Nocodazole	Sigma-Aldrich	Cat# M1404
MG132	Sigma-Aldrich	Cat# C2211
RO-3306	Sigma-Aldrich	Cat# SML0569
Apcin	Boston Biochem	Cat# I-444
proTAME	Boston Biochem	Cat# I-440
Puromycin dihydrochloride	Wako Pure Chemical Industries	Cat# 160-23151
G-418 solution	Roche	Cat# 04727894001
Hygromycin B	Wako Pure Chemical Industries	Cat# 084-07681
Blasticidin S hydrochloride	Funakoshi Biotech	Cat# KK-400
Doxycycline hyclate	Sigma-Aldrich	Cat # D9891
3-Indoleacetic acid (IAA)	Wako Pure Chemical Industries	Cat # 098-00181
DirectPCR® (cell)	Viagen Biotech	Cat #302-C
Antibodies		
Anti- α -tubulin (clone DM1A)	Sigma-Aldrich	Cat# T9026; RRID:AB_477593
Rabbit polyclonal anti-NuMA	Abcam	Cat# ab36999; RRID:AB_776885
Rabbit polyclonal anti-RCC1	Cell Signaling Technology	Cat# 5134
Mouse monoclonal anti-RanGAP1	Santa Cruz Biotechnology	Cat# sc-25630
Mouse anti-importin- β	GeneTex	Cat# GTX22811
Rabbit anti-importin- α	Novus biologicals	Cat# NBP1-31098
Anti-HURP	Nigg lab	N/A
Sheep anti-mouse IgG-HRP	GE Healthcare	Cat# NA931
Donkey anti-rabbit IgG-HRP	GE Healthcare	Cat# NA934
Software and Algorithms		
Photoshop CS5, version 12.0	Adobe Systems	https://www.adobe.com
Fiji	53	https://fiji.sc/
Metamorph	Molecular Devices	https://www.moleculardevices.com
GraphPad Prism 6, version 6.0c	GraphPad Software	https://www.graphpad.com
Excel	Microsoft	https://www.microsoft.com/microsoft-365

RESOURCE AVAILABILITY

Lead Contact

Further information and requests for resources and reagents should be directed to and will be fulfilled by the Lead Contact, Tomomi Kiyomitsu (tomomi.kiyomitsu@oist.jp).

Materials Availability

Plasmids generated in this study will be deposited to Addgene.

Data and Code Availability

This study did not generate/analyze any datasets.

EXPERIMENTAL MODEL AND SUBJECT DETAILS

Established human tissue culture cell lines, and sequence information about guide RNA and PCR primers used in this study are described in [Tables S1–S3](#), respectively.

METHOD DETAILS

Plasmid Construction

Plasmids for CRISPR/Cas9-mediated genome editing and auxin-inducible degron were constructed according to protocols of Natsume et al.³⁶ and Okumura et al.²⁰ To construct donor plasmids containing homology arms for RCC1 (~500-bp homology arms), RanGAP1 (~500-bp), importin- β (~500-bp), HURP (~200-bp), TPX2 (~200-bp), and HSET (~200-bp), gene synthesis services from Eurofins Genomics K.K. (Tokyo, Japan) or Genewiz (South Plainfield, NJ) were used. Plasmids and sgRNA sequences used in this study are listed in [Tables S1](#) and [S2](#), and will be deposited in Addgene.

Cell Culture, Cell Line Generation, and Antibodies

HCT116 cells were cultured as described previously.²⁰ Knock-in cell lines were generated according to procedures described in Okumura et al.²⁰ To activate auxin-inducible degradation, cells were treated with 2 $\mu\text{g}/\text{mL}$ Dox and 500 μM indoleacetic acid (IAA) for 20–24 hr. Cells with undetectable signals for mAID-fusion proteins were analyzed. In the AID system, the target proteins are not degraded in a small population of the cells even in the presence of Dox and IAA, possibly due to the heterogeneous induction of OsTIR1. We took advantages of this to compare two neighboring cells with or without target proteins in the same field in [Figures S2F](#), [S3A](#), [5D](#), and [5G](#).

Flip-In T-REx 293 cells were used in [Figures S2L](#) and [S2M](#) to express mCherry-tagged importin- α constructs. Cell lines were created according to procedures described in Kiyomitsu et al.⁵⁴ To induce transgenes, cells were incubated with 1 $\mu\text{g}/\text{mL}$ tetracycline (MP Biomedicals). Cell lines and primers used in this study are listed in [Tables S1](#) and [S3](#), respectively.

Cell concentrations were determined using the BIO-RAD TC20 Automated Cell Counter (standard protocol). Cells were diluted to a final concentration of 100,000 cells/ml in medium and transferred to 6-well plates for subsequent counting at 24, 48 and 72 hr. Cells were cultured in 4 independent wells and counted twice from each well using the TC20 cell counter.

Antibodies against tubulin (DM1A, Sigma-Aldrich, 1:2,000), NuMA (Abcam, 1:1,000), RCC1 (Cell Signaling Technology, D15H6, Rabbit mAb, 1:100), RanGAP1 (Santa Cruz Biotechnology, H-180, 1:200), importin- β (GeneTex, 3E9 Mouse mAb, 1:100), and HURP (E. Nigg laboratory, 1:200) were used for western blotting. For RCC1 immunoblots, membranes were incubated with anti-RCC1 antibody overnight at 4°C.

Microscope System

Imaging was performed using spinning-disc confocal microscopy with a 60 \times 1.40 numerical aperture objective lens (Plan Apo λ , Nikon, Tokyo, Japan). A CSU-W1 confocal unit (Yokogawa Electric Corporation, Tokyo, Japan) with five lasers (405, 488, 561, 640, and 685 nm, Coherent, Santa Clara, CA) and an ORCA-Flash 4.0 digital CMOS camera (Hamamatsu Photonics, Hamamatsu City, Japan) were attached to an ECLIPSE Ti-E inverted microscope (Nikon) with a perfect focus system. DNA images in [Figures S2D](#) and [S2E](#) or [S3A](#) were obtained using a SOLA LED light engine (Lumencor, Beaverton, OR).

Immunofluorescence and Live Cell Imaging

For immunofluorescence in [Figure S1K](#), HURP-mACF cells were fixed with PBS containing 3% paraformaldehyde and 2% sucrose for 10 min at room temperature. Fixed cells were permeabilized with 0.5% Triton X-100 for 5 min on ice, and pretreated with PBS containing 1% BSA for 10 min at room temperature after washing with PBS. Importin- β was visualized using anti-importin- β antibody (1:500). Images of multiple z sections were acquired by spinning-disc confocal microscopy using 0.5- μm spacing and camera binning 2. Maximally projected images from 3 z sections are shown.

For live cell imaging, cells were cultured on glass-bottomed dishes (CELLview, #627860 or #627870, Greiner Bio-One, Kremsmünster, Austria) and maintained in a stage-top incubator (Tokai Hit, Fujinomiya, Japan) to maintain the same conditions used for cell culture (37°C and 5% CO₂). In most cases, three to five z section images using 0.5- μm spacing were acquired and single z section images are shown, unless otherwise specified. Microtubules were stained with 50 nM SiR-tubulin or SiR700-tubulin (Spirochrome) for > 1 hr prior to image acquisition. DNA was stained with 50 ng/mL Hoechst® 33342 (Sigma-Aldrich) or 20 nM SiR-DNA (Spirochrome) for > 1 hr before observation. To visualize SNAP-tagged HURP, cells were incubated with 0.1 μM TMR-Star (New England BioLabs) for > 2 hr, and TMR-Star were removed before observation. To optimize image brightness, the same linear adjustments were applied using Fiji and Photoshop.

Prometaphase Depletion Assay and Nocodazole Washout

To degrade mAID-tagged proteins during nocodazole arrest, cells were treated with 2 $\mu\text{g}/\text{mL}$ Dox and 3.3 μM nocodazole at the indicated times ([Figure 3A](#)). Five hours after addition of nocodazole, cell culture dishes were moved to the stage of a microscope equipped with a peristaltic pump (SMP-21S, EYELA, Tokyo Rikakikai). Two z section images were acquired using 2- μm spacing at three different (X.Y) positions and at 5-min intervals, with 500 μM IAA added during the first interval. After 90 min, the

nocodazole-containing medium was completely replaced with fresh medium using the peristaltic pump at a velocity of 20 s/mL for 15 min. Images were acquired for a further 2 hr and maximum intensity projection images are shown in [Figures 3B](#) and [3C](#). To analyze spindle orientation in [Figure S3F](#), we took five z section images using 2- μ m spacing. When both spindle poles are included within three z section images, we judged the spindle as having parallel orientation. In [Figure S3D](#), as the largest SiR-tubulin signal in the center of the cell represents centrosomal microtubules, we defined other SiR-tubulin dots on chromosomes as chromosomal microtubule dots and counted the number in the RCC1 positive and negative cells.

Metaphase Depletion Assay

To degrade mAID-tagged proteins in metaphase-arrested cells, cells were treated with 50 μ M Apcin (I-444, Boston Biochem) and 20 μ M proTAME (I-440, Boston Biochem) at the indicated times ([Figure 6C](#)). Three z section images were acquired using 1- μ m spacing at six different (X,Y) positions and at 5-min intervals, with 500 μ M IAA added during the first interval. Maximum intensity projection images are shown in [Figures 6D](#), [7A](#), and [7E](#).

Cold Treatment Assay

To increase the number of cells in metaphase, cells were treated with 20 μ M MG132 (C2211, Sigma-Aldrich) for 90 min. To visualize SNAP-tagged HURP, cells were incubated with 0.1 μ M TMR-Star (S9105S, New England BioLabs) for at least 30 min. Before fixation, cells were incubated in ice-cold medium for 20 min³² to depolymerize non-kinetochore microtubules.

FRAP

FRAP was conducted with a microscope (LEM 780, Carl Zeiss MicroImaging, Inc.), using a 63 x objective lens. Images were acquired every 5 s before and after photobleaching. The bleached area (BA) was set as it covers half spindle and illuminated at $t = 0$ using 560 nm laser (20 mW) with the following setting: speed 4.0 and iteration 1. Metaphase cells that orient parallel to the bottom cover-glass were selected. HURP (TMR-Star) intensity of BA was normalized using the intensity of non-bleached area (NBA) that covers the remaining half spindle. Corrected relative intensity at time t_n was calculated as $(BA_n - BG_n) / (BA_{-1} - BG_{-1}) \times (NBA_{-1} - BG_{-1}) / (NBA_n - BG_n)$, where $t = -1$ represents the first time point of image acquisition before bleaching. BG means background.⁵⁵ Curve fitting and analyses shown in [Figure S6](#) were performed using Fiji.⁵³

QUANTIFICATION AND STATISTICAL ANALYSIS

Quantification of Fluorescent Intensities

To quantify fluorescent intensities of SAFs and SiR-tubulin signals, line scans were performed in Fiji. A 15-pixel-width line was drawn on 16-bit images as it passed on both spindle poles, and peak values were recorded as polar intensities after background subtraction. To analyze intensities on k-fibers, segmented lines with 3-pixel-width were manually drawn on the k-fibers in tubulin images, and then the lines were transferred to SAF images to quantify their signal intensities. To quantify RCC1 intensities on prometaphase chromosomes in [Figure 3D](#), chromosome regions were manually defined with SiR-DNA images, and the regions were transferred to RCC1 images to quantify the intensities.

Statistical Analysis

To determine the significance of differences between the mean values obtained for two experimental conditions, Welch's t tests (Prism 6; GraphPad Software, La Jolla, CA) were used. One-way ANOVA was performed in [Figures 1D](#), [2F](#), and [S7L–S7N](#) using Prism 6. For all Figures: error bars indicate mean \pm SD; * $p < 0.05$, ** $p < 0.01$, *** $p < 0.001$, **** $p < 0.0001$; scale bars = 10 μ m.